Applied Surface Science 256 (2009) 1582–1588

Contents lists available at ScienceDirect

Applied Surface Science

journal homepage: www.elsevier.com/locate/apsusc

Analysis of oxide formation induced by UV laser coloration of stainless steel

Z.L. Li [a,*], H.Y. Zheng [a], K.M. Teh [a], Y.C. Liu [a], G.C. Lim [a], H.L. Seng [b], N.L. Yakovlev [b]

[a] Singapore Institute of Manufacturing Technology, 71 Nanyang Drive, 638075, Singapore
[b] Institute of Materials Research and Engineering, 3 Research Link, 117602, Singapore

ARTICLE INFO

Article history:
Received 31 May 2009
Received in revised form 2 September 2009
Accepted 9 September 2009
Available online 17 September 2009

Keywords:
Laser color marking
Stainless steel oxidation
Element diffusion

ABSTRACT

Laser-induced coloration on metal surfaces has important applications in product identification, enhancing styles and aesthetics. The color generation is the result of controlled surface oxidation during laser beam interaction with the metal surfaces. In this study, we aim to obtain in-depth understanding of the oxide formation process when an UV laser beam interacts with stainless steel in air. The oxide layer is analysed by means of optical microscopy, scanning electron microscopy (SEM) and time-of-flight secondary ion mass spectrometer (TOF-SIMS). TOF-SIMS results clearly show the formation of duplex oxide structures. The duplex structure includes an inner layer of Cr oxide solution and an outer layer of Fe oxide solution. The oxide layer thickness increased as the results of Fe diffusion to surface during multiple laser scanning passes.

1. Introduction

Printing and emulsion coating techniques are conventionally used to achieve color markings on metal surfaces. Scratch and wear of such coatings and the fading of colors with time are recognized problems associated with these coatings. Decorative coatings on metal surfaces may also be prepared by electrochemical treatment in aqueous electrolytes. In these processes, changing the metal ions in the electrolyte produces different colors on the metal surface [1]. The flexibility of obtaining different colors and patterns is limited.

Traditional laser marking is achieved by engraving patterns or texts on products or component surfaces and has found many applications in making personalized gifts, security identification, surface textures, product serialization, copyright patterns, etc. The digital nature of laser engraving allows a great variety of individual customizations. However, these are typically monochromatic marks that are functional but often lack of aesthetic appeal compared with color marking. Laser coloring metals have been demonstrated by two major mechanisms. Firstly, the laser, such as Excimer and CO_2 laser, acts as a heating source, which produces transparent oxide films on the metal surface when it is exposed in air or oxygen atmosphere. Uniform and high contrast colors on metal surfaces were obtained under different process conditions [2–5]. Colors are produced as a result of constructive or destructive interference depending on the film property at a given beam light incidence angle. When the film is illuminated by white light, its color at any point is formed by the mixture of those wavelengths that are reflected and interfered constructively. The color for the reflected wavelength that interfered destructively will be absent [6]. Secondly, colors have been generated on various metal surfaces, such as Ag, Au, Al, Pt, using femto- and picosecond lasers surface structuring technique [7–10]. In these studies, nano-protrusions are realized on surface. The color is determined by the position of the plasmon resonance of the free electrons in the nano-relief.

Recently, O'Hana demonstrated that laser beam can be used as a colorful "pen" by artists for fashion metal jewellery design [11]. The work delivers a message that engineering and art are synergistic. To obtain a wide spectrum of colors, the key factor is to control the formation of metal oxides with desired thickness and optical properties if thin film interference leads the color generation. Although there are reports in laser color marking on metal surfaces [2,12], detailed analyses of the laser-induced oxide formation are not available. Being one of the most widely used alloys, stainless steel and its color marking process has wide potential applications in fashion jewellery, souvenirs, product identification and tracking.

This paper reports a study on photothermal oxidation of stainless steel using a solid state UV laser. By analysing the laser marked areas with TOF-SIMS, the results clearly show the formation of duplex oxide structures that are formed with differing complexity depending on laser marking parameters. The duplex structure includes an inner layer of Cr oxide solution and an outer layer of Fe oxide solution. It is identified that the concentration and depth profiles of Cr and Fe oxides changes with the number of laser scanning passes. The oxide layer thickness increased as the results of Fe diffusion to surface during multiple laser scanning process.

* Corresponding author. Tel.: +65 6793 8417; fax: +65 6791 6377.
E-mail address: zlli@SIMTech.a-star.edu.sg (Z.L. Li).

0169-4332/$ – see front matter © 2009 Elsevier B.V. All rights reserved.
doi:10.1016/j.apsusc.2009.09.025

2. Experimental

Q-switched third-harmonic Nd:YVO_4 laser with a wavelength of 355 nm was used for conducting the experiments in air. The laser beam pulse width was about 25 ns. The scanning speed of the laser beam was set between 400 and 500 mm/s with laser power from 7 to 10 W at a frequency of 40 kHz. The beam was focused to a spot size of 13 μm using an f-theta lens with effective focal length (EFL) of 108.3 mm. The laser beam was directed using a galvanometric scanner to raster scan an area of 2 mm × 2 mm. The raster spacing between the scanning laser beam was set at 30 μm. In order to eliminate ablation, the beam intensity was reduced by focusing it at a plane 3–3.5 mm below the sample surface. The width of the laser marked trace was measured as about 85–90 μm. The number of scan passes over the same area was varied from one to six. The microstructures of laser scanned samples were examined by means of an Axiotron 2 inspection optical microscope and a Zeiss EVO 50 scanning electron microscope (SEM). The thickness and composition of the oxides were analysed by time-of-flight secondary ion mass spectrometer (TOF-SIMS). The area of SIMS analysis was 150 μm × 150 μm. The sputtering rate was calculated as 0.9 nm/s, which was the result of the crater depth divided by the sputtering time. The value of the sputtering rate was used for calculating the oxide thicknesses. The crater depths generated during ion sputtering were measured using a Taylor–Hobson Stylus Profilometer. The accuracy of the Profilometer was 20 nm. Stainless steel 304, an austenitic stainless, was used for the study. The atomic ratios of major elements were detected using EDX as Fe: 69.4%, Cr: 19.1%, Ni: 7.8%, Mn: 1.5%, and Si: 2.2%. Alloying element ratios in the oxide layers were calculated by multiplying each ion intensity with a coefficient. The coefficient was calculated by normalizing the ion intensity to the sum of the major elements such that the composition close to the expected steel composition at the base metal was obtained.

3. Results

3.1. Laser-induced colors on stainless steel

Laser-induced color patterns on a stainless steel are shown in Fig. 1. The colors were produced by varying laser power, focal plane offset, and scanning direction as indicated in the figure. Raster scanning spacing, scanning speed and number of passes were kept constant as 30 μm, 400 mm/s and 4 passes, respectively. It is clearly shown that the color produced on stainless steel is very sensitive to the laser parameters. The power and focal plane offset determine the laser power density delivered to the surface, and thus affect the surface temperature and degree of oxidation. However, the effect of scanning direction is not clear. Further study is needed to clarify this phenomenon.

Typical experiments were carried out to further investigate photochemical oxidation of the sample during laser processing. In following sections, all laser experimental parameters are set as: laser power 10 W, focal plane at 3.5 mm below the sample surface. Scanning speed and number of scanning passes are varied.

3.2. Optical microstructures relating to the number of laser scan passes

When observed under an optical microscope, Fig. 2(a) shows the optical micrograph of as-received stainless steel sample surface before being treated with the laser beam. Scratches were clearly observed on the sample surface. The sample was then scanned with the laser beam at a scanning speed of 500 mm/s. Three areas were scanned with one, two and three passes, respectively. The optical micrographs of the three areas are shown in Fig. 2(b–d). The scanned areas clearly showed coloration and morphology changes according to different number of laser scanning passes. This indicated that the microstructures of the thin oxide films gradually altered due to formation of new oxide phases or phase composition changes after each laser scan pass. No further microstructure changes were observed after three laser scan passes.

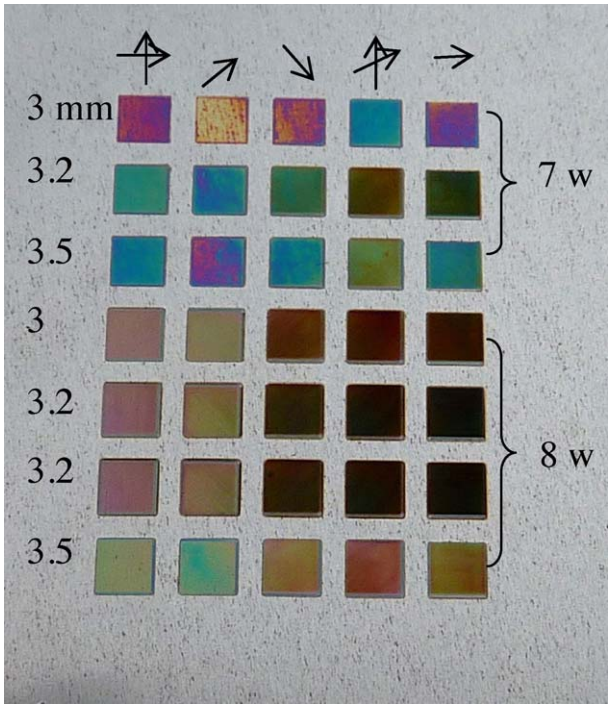

Fig. 1. Laser produced colors on stainless steel at various processing parameters.

3.3. Optical microstructure relating to laser beam scanning speed

Figs. 2(b) and 3 show micrographs of the samples after one laser scan pass at the speeds of 500 mm/s and 400 mm/s, respectively. For the sample scanned at the speed of 500 mm/s, three major microstructures were observed, namely irregular islands with different shapes and sizes, dark spots within the large islands, and the base metal. It is known that oxidation reaction took place during laser processing in air. The island microstructures were likely made of discontinuous oxides formed during rapid heating by the laser beam. The dark spots were likely due to Cr precipitates during the oxidation process [13]. SEM observation supported the above conclusion as shown in Fig. 4(a) where two contrasting microstructures appeared: bright islands and dark base. Metal oxide is a semiconductor which shows brighter contrast than its base metal due to its poorer electrical conductivity. Subsequent laser scanning passes generated continuous oxide film as evidenced by the disappearing of the island microstructures, as shown in Figs. 2(c and d) and 5. When the laser beam scanning speed was reduced to 400 mm/s, another type of irregular structures appeared but with significantly smaller quantity as shown in Fig. 3. It is believed that continuous oxide layer was formed under this process condition. The smaller quantities of islands are most likely due to randomly distributed un-oxidized base metal in the oxide matrix. Fig. 4(b) shows that brighter oxide phase is dominant at the surface.

3.4. TOF-SIMS analysis

3.4.1. Depth of the oxide layer

Fig. 6 shows the SIMS depth profiles of the oxides after laser scan passes of 1, 2 3 and 6 passes at a speed of 500 mm/s. Three

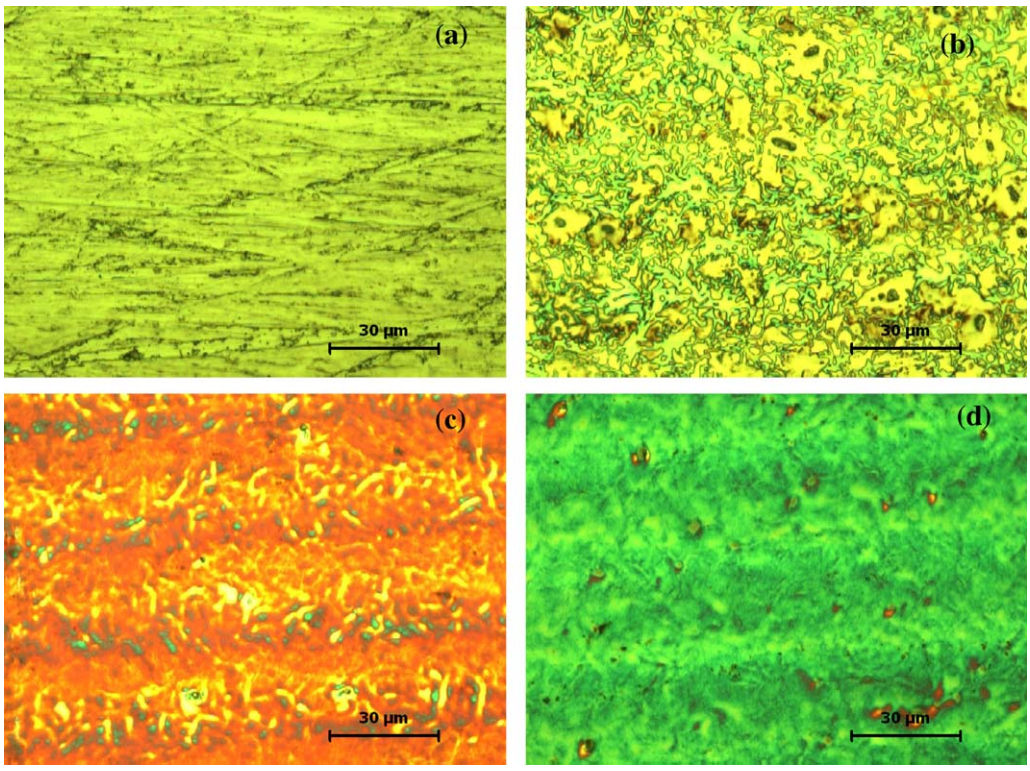

Fig. 2. Optical micrographs of the samples for (a) as-received, and laser scans at (b) one pass, (c) two passes, and (d) three passes. Laser parameters: power 10 W, scanning speed 500 mm/s.

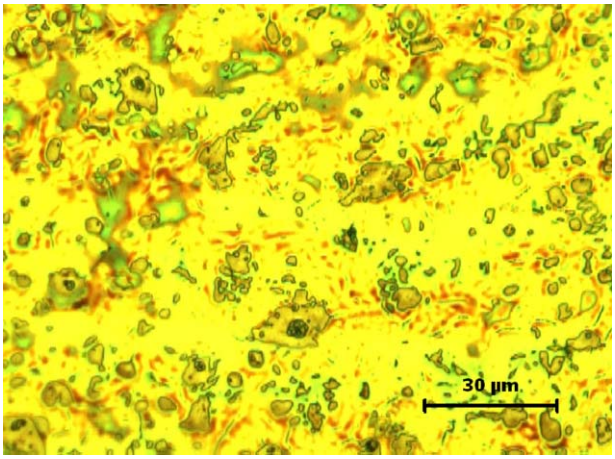

Fig. 3. Optical micrograph of the sample after one laser scan pass at power 10 W and scanning speed of 400 mm/s.

sub-layers were revealed as seen in Fig. 6(b): (1) oxide I layer in which the O counts remained at relatively constant level. The Ni and Si counts decreased from the surface to their lowest levels at the bottom of the oxide I layer. Mn counts decreased and started to form an upward turn at the interface between oxide I and oxide II. (2) Oxide II layer where the O counts started to decrease till zero. The Ni and Si counts increased from their minima to maxima through the oxide II layer. Mn completed the upward turn. (3) Interface layer in which O was not detected while other element counts including Fe, Cr, Ni, Mn and Si decreased to the same levels as the base metal. The thicknesses of each layer are shown in Table 1.

The oxide I layer was not detected after one laser scan pass at the speed of 500 mm/s as shown in Fig. 6(a). Only oxide II and interface layers were observed. Fig. 6(b) shows that the oxide I layer was formed after two laser scan passes and its thickness rapidly increased to 169 nm. The oxide I layer growth rate slowed down to 30 nm/pass in the third and fourth scan pass and further reduced to 4–5 nm/pass in the fifth and sixth. The thickness of the

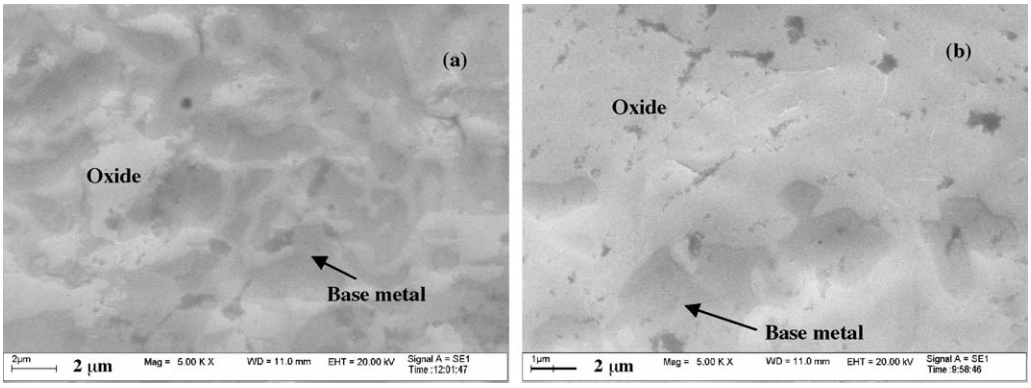

Fig. 4. SEM micrographs of the samples after one laser scan pass at power 10 W and scanning speed of (a) 500 mm/s and (b) 400 mm/s.

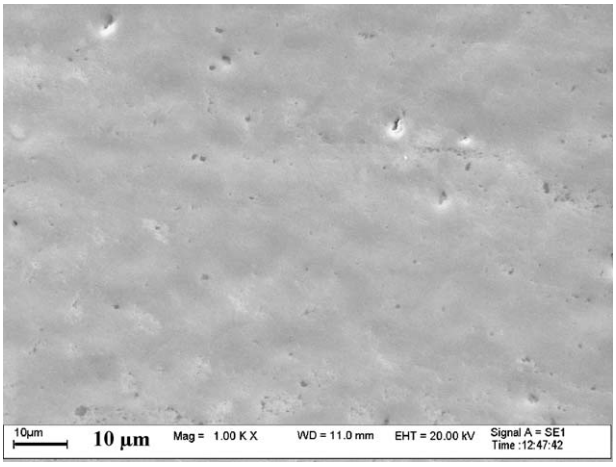

Fig. 5. SEM micrograph of the sample after two laser scan passes at power of 10 W and scanning speed of 500 mm/s.

oxide II layers were found to decrease with increasing number of laser scan passes. This may indicate a partial conversion from oxide II to oxide I. No clear trends were observed for the thicknesses of the interface layers when the number of laser scan passes was varied. Possible measurement errors may arise due to the high fluctuations in SIMS counts at the interfaces.

At the scanning speed of 400 mm/s, oxide I layer was formed after one laser scan pass as shown in Fig. 7. The depth profiles of two to six scan passes were similar to those shown in Fig. 6 and therefore are not show here. The oxide I layer rapidly grew to 118 and 184 nm after the first and second laser scan pass and reached a thickness of about 213 and 229 nm after the third and fourth pass with the growth rate reduced to 16–19 nm/scan. Oxide I layer thickness remained the same in the fifth and sixth scan passes. No clear trends were observed for the thickness of oxide II and the interface layers when the numbers of laser passes were varied. The above observations showed that the oxide I layer grew rapidly during the first and second scan pass and slowed down in the third and fourth. For the fifth and sixth passes, the oxide I thickness became stable in the sample scanned at 400 mm/s while it still grew slowly in the sample scanned at 500 mm/s.

3.4.2. Oxide layer morphology

It is known that SIMS sputtered craters have slanted wall. Fig. 8 shows the top views of the slanted oxide walls. After one laser pass at a speed of 500 m/s, a barely perceptible band between the oxide and base metal was observed as shown in Fig. 8(a). Discontinuous oxides grew from the surface into the depth in the band. No clear interface between the oxide and base metal was found. Fig. 8(b–d) shows the micrographs of the samples after 2, 3, and 6 laser scan passes. Three sub-layers were observed as red and yellow bands followed by a zigzag bold line in between the oxide and base metal. The red and yellow bands were likely images of the slanted oxides, which have different optical properties. It will be discussed in next section that the oxide contains a duplex structure (inner "Cr_2O_3" and outer "Fe_2O_3"). The interfaces between the two oxide layers were not uniform as shown in Fig. 8. The zigzag lines represented the interface between oxide and base metal. The interface was

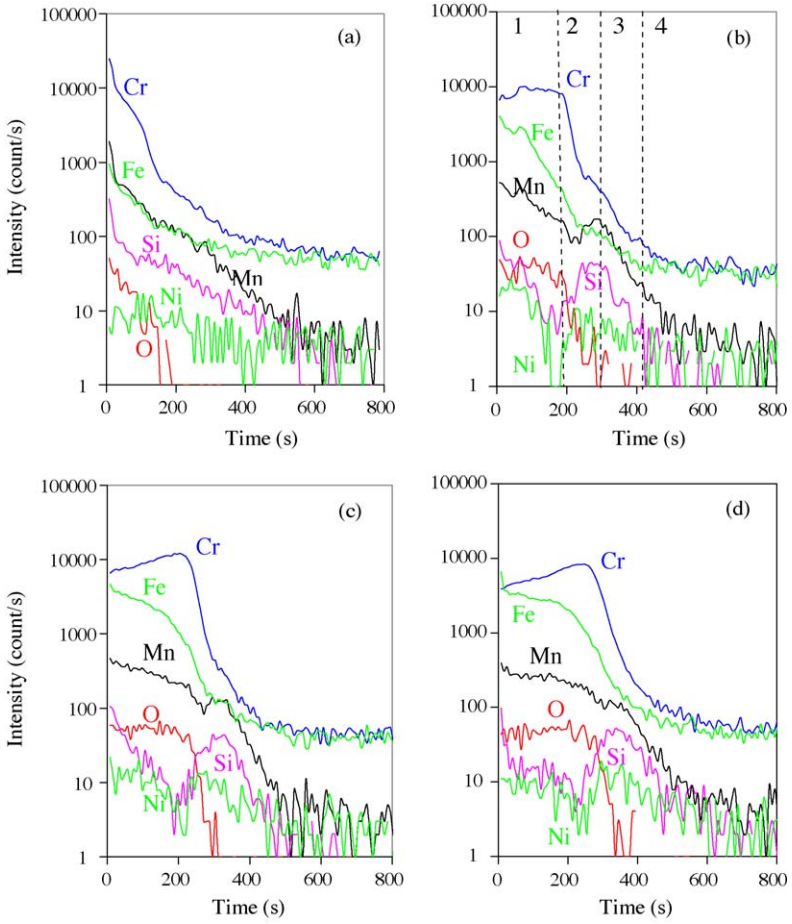

Fig. 6. TOF-SIMS depth profiles of the samples after laser scans of (a) one passes, (b) two passes, (c) three passes, and (d) six passes. The numbers on (b) denote the sub-layers. Laser parameters: power 10 W, scanning speed 500 mm/s.

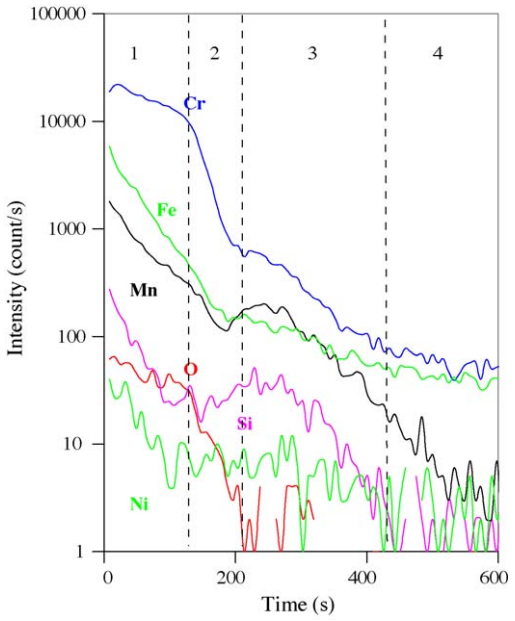

Fig. 7. TOF-SIMS depth profiles of the sample after one laser scan pass. Laser parameters: power 10 W, scanning speed 400 mm/s.

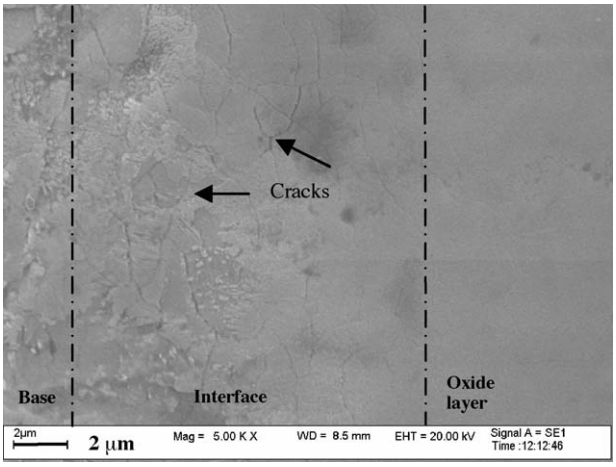

Fig. 9. SEM micrograph at the edge of SIMS crater. Laser parameter: power 10 W, scanning speed 500 mm/s, two scan passes.

rough after two laser passes and gradually became smoother as the numbers of passes increased. However, no straight interface was observed after six laser passes. These observations suggested that the thickness of the laser-induced oxides were not uniform.

Fig. 9 shows the SEM micrograph of the interfaces between oxide/base metal in the SIMS crater after two laser scan passes at a speed of 500 mm/s. It was observed that the base metal in the crater was rough after the ion sputtering as compared to the smooth oxide layer. No microcracks were found in the oxide layer under SEM with 5000 times magnification. Microcracks appeared at the interface after two laser passes, and the orientations of the majority of microcracks were parallel to the interface. The amount and size of the microcracks were found to increase with the numbers of laser passes. It was discussed in the previous section that the oxide layer grew rapidly at the first and second laser passes. The growth slowed down at the third and subsequent passes which coincide with microcracks formation at the oxide/base metal interface. The formation mechanism of microcracks is not clear. It might be attributed to the stress developed due to

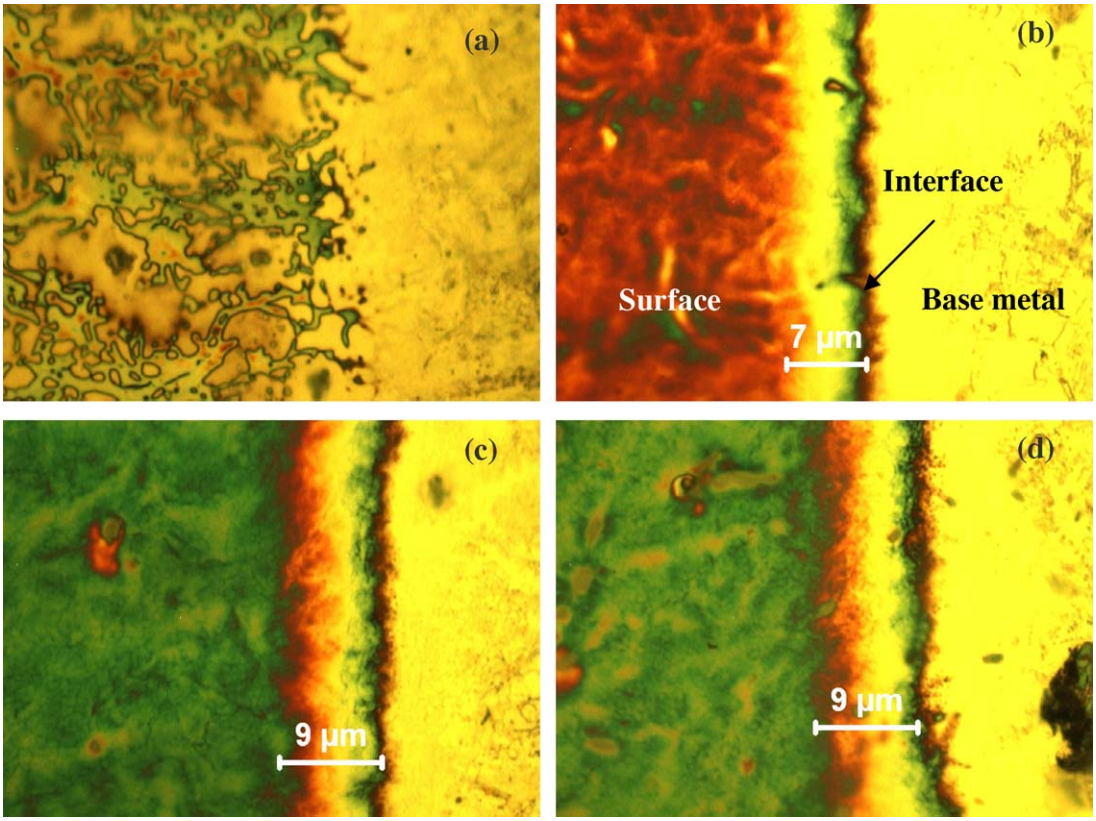

Fig. 8. Optical micrographs of the edges of SIMS craters. Laser scan passes were (a) one, (b) two, (c) three, and (d) six. The laser parameters: power 10 W and scanning speed 500 mm/s.

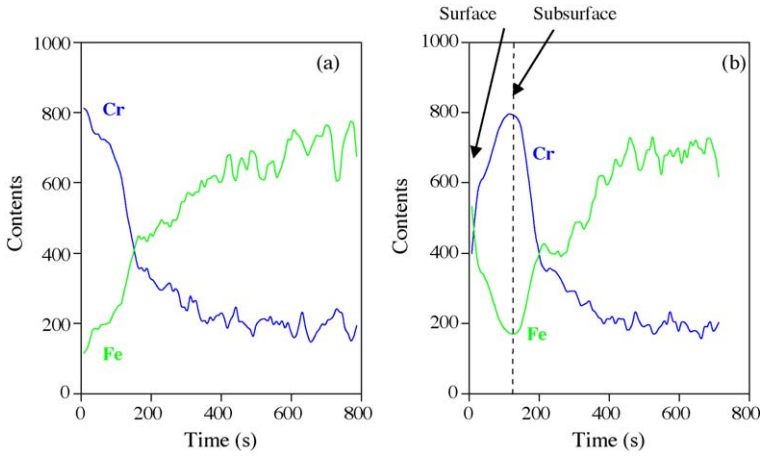

Fig. 10. Cr:Fe ratio in the laser-induced oxide layer. One scan pass at a scanning speed of (a) 500 mm/s and (b) 400 mm/s. Laser parameters: power 10 W.

Table 1
Oxide depths obtained at various laser process conditions.

Number of passes	500 mm/s				400 mm/s			
	Oxide I (nm)	Oxide II (nm)	Total oxide (nm)	Interface (nm)	Oxide I (nm)	Oxide II (nm)	Total oxide (nm)	Interface (nm)
1	–	140	140	213	118	88	206	192
2	169	95	264	125	184	60	244	221
3	191	96	287	140	213	67	280	273
4	228	67	295	149	229	88	317	176
5	221	89	310	125	221	59	280	133
6	236	66	302	258	229	104	333	88

volume change during oxide growth [14]. The microcracks might become barrier to ions diffusion which impeded oxide growth in subsequent laser scanning passes.

3.5. Discussions

Single photo-dissociation energy of oxygen may occur at around 5.1 eV which corresponds to a wavelength λ, of 240 nm. The wavelength of the laser used in this experiment was 355 nm and hence likely the mechanism that caused the changes in the irradiated areas was the thermal energy from the laser beam. In pulsed laser process with fast moving beam, the total energy E absorbed by a spot can be calculated by pulse energy times the number of pulses delivered to the spot: $E = (P/RR) \times (D \times RR/v) = (P \times D/v)$. Where P is laser power, D is beam size, RR is pulse repetition rate, v is laser beam scanning speed. If the cooling cycle of a pulsed beam is ignored, the surface temperature rise during the process can be simply described by: $\Delta T \approx [E/(c \times \rho)] = [(P \times D)/(v \times c \times \rho)]$ [15], c and ρ is specific heat and mass density of the material, respectively. A faster scanning speed results in lower surface temperature. Furthermore, a faster scanning speed reduces the laser beam-material interaction time which is unfavorable to diffusion of elements within the heated layer. In order to understand the effects of the scanning speed on diffusion of elements in the oxide layer during laser process, the SIMS counts of elements were normalized with the base metal. The normalized Fe and Cr contents after one laser scan pass are shown in Fig. 10. When laser scans at the speed of 500 mm/s, Fig. 10(a) shows that the ratio of Cr:Fe contents was about 7:1 as comparing to the 0.28:1 in the base metal. The result indicated that chemisorbed O selectively reacts with Cr ions/atoms producing an ultrathin oxide, "Cr_2O_3", on the surface due to Cr having higher affinity for O. The quotation marks indicate that the oxide is doped with small quantities of alloy elements Fe, Ni, Si and Mn. The oxide was formed at where Cr was richer due to insufficient diffusion time for the Cr to come to the surface, leading a discontinuous oxide islands. When laser beam scans at the speed of 400 mm/s, Fig. 10(b) shows the ratio of Cr:Fe contents at the surface were about 0.75:1, which is closer to the base metal composition of 0.28:1. The Cr concentration increased to a Cr:Fe ratio of 4.6:1 at the subsurface. A duplex structure was formed which consisted of an inner layer of Cr oxide solution "Cr_2O_3(Fe)", and an outer layer of Fe oxide solution "Fe_2O_3(Cr)" [16]. The quotation marks indicate that the oxide solutions were doped with small quantities of alloy elements

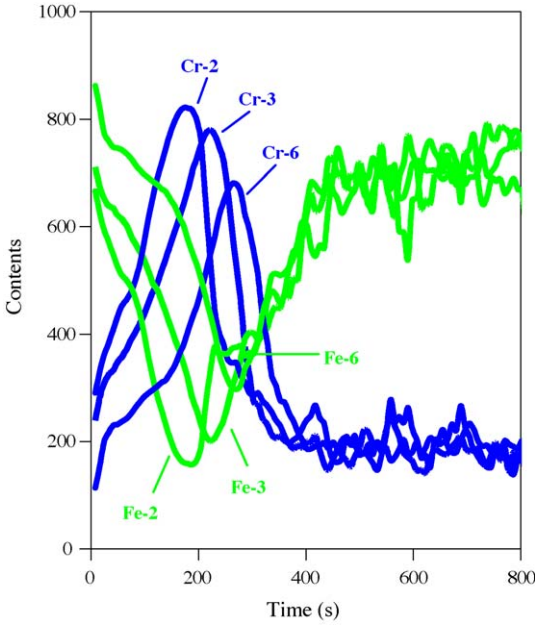

Fig. 11. Cr:Fe ratio in the laser-induced oxide layer. Laser parameters: power 10 W, scanning speed 500 mm/s. The numbers denote the number of laser scan passes.

Ni, Si and Mn. The result implies three possibilities: (1) both Fe and Cr reacted with O at same time under this laser process condition due to the sufficient high temperature enable Fe competing with Cr in reaction with O at the interface of air-metal. (2) Selective Cr oxidation takes place first and Fe diffuses through the ultrathin "Cr_2O_3" to form "Fe_2O_3" on the surface. (3) Both of above reactions take place. The concentration of Cr at the subsurface indicates that Fe diffusion occurs. Therefore, the second and third possibilities are more likely.

Subsequent laser scan passes resulted in more Fe diffused to the outer surface to react with O for both scanning speeds. Fig. 11 shows the results obtained at the laser scanning speed of 500 mm/s. The results at scanning speed 400 mm/s has similar behavior therefore is not shown here. The ratio of Cr:Fe at the surface rapidly reduced to 0.43:1 after two scan passes, and to 0.33:1 and 0.13:1 after three and six passes, respectively. Cr was concentrated at the subsurface where the maximum ratios of Cr:Fe were 5.1:1, 3.9:1 and 2.3:1 after two, three and six passes, respectively. The corresponding locations of the maximum ratios of Cr:Fe were 155, 199 and 236 nm, respectively, which were about the same depth of the oxide I layers, as shown in Table 1. The observations suggested that the oxide growth was the result of Fe diffusion though the existing oxide during the multiple laser beam scan passes and the compositions in the duplex structure gradually altered. At the inner layer Cr oxide solution tended to form spinel oxide $FeFe_{2-x}Cr_xO_4$, where $0 < x < 2$. The Fe oxide solution at the outer surface tended to become purer Fe oxide. The stratify scale may be still protective due to presence of Cr at the outer layer [16]. Corrosion tests showed that the oxide was durable after a 30 min ultrasonic rinsing in various solutions including alcohol, acetone and diluted acids and alkaline [2]. In our lab, the colors induced by laser irradiation on stainless steel remained stable after 3 years exposure in air with 80% humidity.

4. Conclusions

UV laser-induced coloration and photothermal oxidation of stainless steel is studied. The results clearly show that the colors produced by laser irradiation are very sensitive to laser energy density delivered to the surface. The colors are affected by key processing parameters including laser power, focal plane offset, scanning direction and scanning speed. Further studies find that initial oxidation reaction is affected by laser scanning speed. In the case of laser beam scanning speed of 500 mm/s, Cr is selectively oxidized at the surface where Cr is rich. In the case of laser beam scanning speed of 400 mm/s, duplex oxide structure is formed, which include inner layer Cr oxide solution and outer layer of Fe oxide solution. The oxide layer thickness increased as the results of Fe diffusion to the surface during multiple laser scanning passes. The compositions of the duplex changes after each laser pass. The Cr content in the outer layer gradually reduces and "purer" Fe oxide is formed after six laser passes. The Fe content in the inner layer gradually increases, spinel oxide is formed after six laser passes. Microcracks are observed at the oxide/base metal interface the amount of which increases with the number of laser scan passes. The oxide growth rate decreases with the numbers of laser passes and their thickness tends to stabilize due to Fe diffusion in the oxide layer being restricted by: (1) longer distance of diffusion through the thicker oxide layer and (2) microcracks at the oxide/base metal interface.

References

[1] P. Kurze, W. Krysmann, M. Berger, K. Rabending, J. Schreckenbach, T. Schwarz, K.-H. Hartmann, Method for the preparation of decorative coating on metals, U.S. Patent No. 4,869,789 (1989).
[2] H.Y. Zheng, G.C. Lim, X.C. Wang, J.L. Tan, Process study for laser-induced surface coloration, J. Laser Appl. 14 (4) (2002) 215–220.
[3] H.Y. Zheng, G.C. Lim, Process for laser marking metal, U.S. Patent No. 09/799724 (2003).
[4] L. Baufay, F.A. Houle, R.J. Wilson, Optical self-regulation during laser-induced oxidation of copper, J. Appl. Phys. 61 (9) (1987) 4640–4651.
[5] S. Gaković, M. Trtica, S. Petrović, P. Panjan, M. Čekada, Z. Samardžija, Surface structures formed on ALSI 420 stainless steel by pulsed laser irradiation, Mater. Sci. Forum 494 (2005) 309–314.
[6] J.A. Richards, F.W. Sears, M.R. Wehr, M.W. Zemansky, Modern University Physics, Addison-Wesley, Reading, 1966.
[7] E.V. Zavedeev, A.V. Petrovskaya, A.V. Simakin, G.A. Shafeev, Formation of nanostructures upon laser ablation of silver in liquids, Quant. Electron. 36 (10) (2006) 978–980.
[8] S. Lau Truong, G. Levi, F. Bozon-Verduraz, A.V. Petrovskaya, A.V. Simakin, G.A. Shafeev, Generation of Ag nanospikes via laser ablation in liquid environment and their activity in SERS of organic molecules.
[9] A.Y. Vorobyev, C.L. Guo, Colorizing metals with femtosecond laser pulses, Appl. Phys. Lett. 92 (2008), 041914(1)–041914(3).
[10] E. Stratakis, V. Zorba, M. Barberoglou, C. Fotakis, G.A. Shafeev, Femtosecond laser writing of nanostructures on bulk Al via its ablation in air and liquids, Appl. Surf. Sci. 255 (2009) 5346–5350.
[11] S. O'Hana, Jewellery design using lasers: an artist's view, Laser User 47 (2007) 32–132.
[12] A. Pérez del Pino, J.M. Fernández-Pradas, P. Serra, J.L. Morenza, Coloring of titanium through laser oxidation: comparative study with anodizing, Surf. Coat. Technol. 187 (2004) 106–112.
[13] A.V.C. Sobral, M.P. Hierro, F.J. Pérez, W. Ristow Jr., C.V. Franco, Oxidation of injection molding 316L stainless steel at high temperature, Mater. Corrosion 51 (2000) 791–796.
[14] G.C. Wood, The oxidation of iron–chromium alloys and stainless steels at high temperatures, Corros. Sci. 2 (1962) 173–196.
[15] D. Bäuerle, Laser Processing and Chemistry, second ed., Springer, New York, 1996
[16] D. Peckner, I.M. Bernstein, Handbook of Stainless Steels, McGraw-Hill Book Company, New York, 1977.